LETTER

doi:10.1038/nature14569

Epoxyeicosatrienoic acids enhance embryonic haematopoiesis and adult marrow engraftment

Pulin Li[1,2]*, Jamie L. Lahvic[1]*, Vera Binder[1,3]*, Emily K. Pugach[1], Elizabeth B. Riley[1], Owen J. Tamplin[1], Dipak Panigrahy[4], Teresa V. Bowman[1], Francesca G. Barrett[1], Garrett C. Heffner[1], Shannon McKinney-Freeman[5], Thorsten M. Schlaeger[1], George Q. Daley[1], Darryl C. Zeldin[6] & Leonard I. Zon[1,2]

Haematopoietic stem and progenitor cell (HSPC) transplant is a widely used treatment for life-threatening conditions such as leukaemia; however, the molecular mechanisms regulating HSPC engraftment of the recipient niche remain incompletely understood. Here we develop a competitive HSPC transplant method in adult zebrafish, using *in vivo* imaging as a non-invasive readout. We use this system to conduct a chemical screen, and identify epoxyeicosatrienoic acids (EETs) as a family of lipids[1,2] that enhance HSPC engraftment. The pro-haematopoietic effects of EETs were conserved in the developing zebrafish embryo, where 11,12-EET promoted HSPC specification by activating a unique activator protein 1 (AP-1) and *runx1* transcription program autonomous to the haemogenic endothelium. This effect required the activation of the phosphatidylinositol-3-OH kinase (PI(3)K) pathway, specifically PI(3)Kγ. In adult HSPCs, 11,12-EET induced transcriptional programs, including AP-1 activation, which modulate several cellular processes, such as migration, to promote engraftment. Furthermore, we demonstrate that the EET effects on enhancing HSPC homing and engraftment are conserved in mammals. Our study establishes a new method to explore the molecular mechanisms of HSPC engraftment, and discovers a previously unrecognized, evolutionarily conserved pathway regulating multiple haematopoietic generation and regeneration processes. EETs may have clinical application in marrow or cord blood transplantation.

To our knowledge, a screen-based forward-genetic approach to understand transplantation biology has never been attempted. In an effort to quantify HSPC activity, we developed a competitive transplantation system in a transparent mutant zebrafish, *casper*[3], which allows direct visualization of engraftment *in vivo*. We co-injected whole kidney marrow (WKM) cells from two ubiquitous GFP and DsRed2 transgenic donors into *casper* (Fig. 1a), and calculated relative engraftment as the ratio of GFP/DsRed2 intensity (*G*/*R*) within the same kidney region (Fig. 1b). We validated the quantitative potential of this imaging-based approach by comparing with flow cytometry-based analysis of WKM from the same recipient (Fig. 1c). The assay was also sensitive to changes in the relative number of green-to-red donor cells (Fig. 1d). Additionally, our system successfully detected the effects of two known chemical modulators of HSPC engraftment: dmPGE$_2$ (16,16-dimethyl-prostaglandin E$_2$), a stabilized derivative of PGE$_2$ (ref. 4), and BIO (6-bromoindirubin-3′-oxime), a GSK-3β inhibitor[5]. We used our assay to screen 480 compounds with known bioactivities, which had been selected to cover diverse signalling pathways (Extended Data Fig. 1a). Ten compounds significantly increased the *G*/*R* ratio reproducibly, including PGE$_2$ and Ro 20-1724, which activates the cAMP pathway downstream of PGE$_2$ (refs 4 and 5). The other hits target pathways that previously have not been linked to HSPC engraftment, including 11,12-EET and 14,15-EET (Fig. 1e). These are arachidonic-acid-derived eicosanoids that are synthesized through the cytochrome P450 epoxygenase pathway[1,2] (Extended Data Fig. 1b).

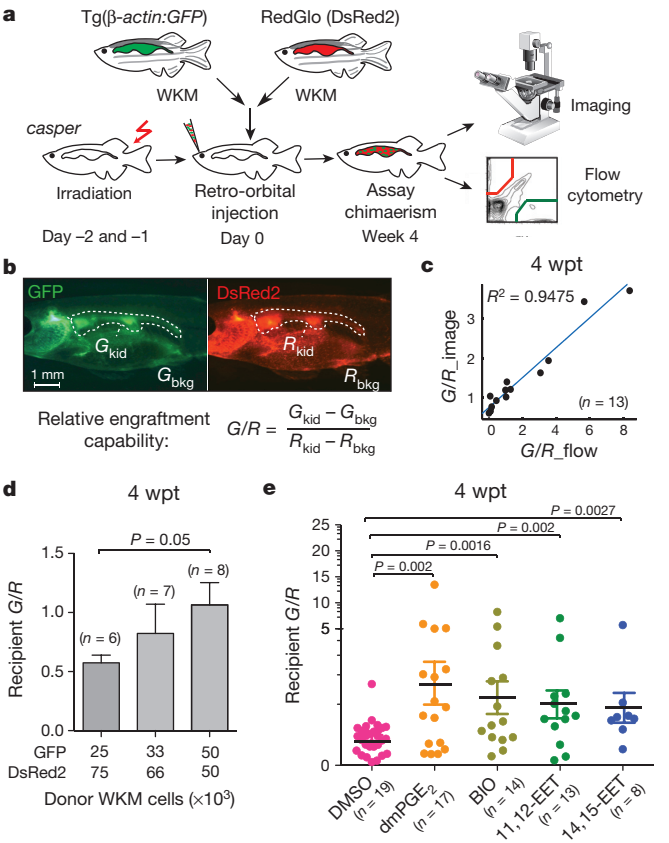

Figure 1 | Zebrafish whole kidney marrow competitive transplantation-based chemical screen identifies EETs as enhancers of marrow engraftment. **a**, Schematic of zebrafish whole kidney marrow (WKM) competitive transplantation. **b**, Calculation of relative engraftment capability (*G*/*R*). White dashed line denotes kidney. G_{kid}/R_{kid}, kidney fluorescence intensity; G_{bkg}/R_{bkg}, background fluorescence intensity. **c**, The *G*/*R* ratios from imaging linearly correlated with flow cytometry analysis of the same recipients (linear regression). wpt, weeks post-transplant. **d**, Serial dilution competitive transplantation with varying donor GFP/DsRed2 ratios. **e**, Four-hour transient chemical treatment increased WKM engraftment. 11,12- and 14,15-EET, 0.5 μM. Unpaired two-tailed *t*-test; mean and s.e.m. (**d**, **e**).

[1]Stem Cell Program and Division of Haematology/Oncology, Boston Children's Hospital and Dana-Farber Cancer Institute, Howard Hughes Medical Institute, Harvard Stem Cell Institute, Harvard Medical School, Boston, Massachusetts 02115, USA. [2]Chemical Biology Program, Harvard University, Cambridge, Massachusetts 02138, USA. [3]Department of Hematology and Oncology, Dr. von Hauner Children's Hospital, Ludwig-Maximilians University, 80337 Munich, Germany. [4]Center for Vascular Biology Research, Beth Israel Deaconess Medical Center, Harvard Medical School, Boston, Massachusetts 02115, USA. [5]Department of Haematology, St Jude Children's Research Hospital, Memphis, Tennessee 38105-3678, USA. [6]Division of Intramural Research, National Institute of Environmental Health Sciences, National Institutes of Health, Research Triangle Park, North Carolina 27709, USA.
*These authors contributed equally to this work.

A gene expression study previously reported mouse *Cyp2j6*, a cytochrome P450 epoxygenase, as one of the 93 genes enriched in long-term haematopoietic stem cells[6].

Despite years of research on the potent effects of EETs in numerous physiological processes[7–9,22], knowledge about their direct target(s) and downstream pathway(s) is still very limited. To tackle this problem, a robust system allowing easy genetic perturbation is crucial. As adult regeneration often reactivates pathways important for development, we decided to probe the effects of EETs on haematopoiesis during embryo development. Analogous to mammalian development, zebrafish HSPCs form from a *flk1*+ population, named haemogenic endothelium, at 24 hours post fertilization (hpf), and become *runx1*+ at 36 hpf in the evolutionarily conserved aorta–gonad–mesonephros (AGM) region[10–12]. HSPCs enter the circulation after they emerge from the AGM[11–13], and seed the caudal haematopoietic tissue (CHT), a secondary haematopoietic site equivalent to the mammalian fetal liver[14,15] (Fig. 2a). The 11,12-EET treatment between 24 and 36 hpf strongly increased the HSPC marker *runx1* in the AGM, and surprisingly induced *runx1* in a non-haematopoietic region of the tail mesenchyme, where *runx1* is not normally expressed (Fig. 2b). This indicates 11,12-EET might be inducing a conserved transcriptional program. We confirmed this AGM phenotype with *in vivo* time-lapse imaging of HSPC birth from the haemogenic endothelium. Tg(*CD41:GFP; flk1:DsRed2*) embryos treated with 11,12-EET starting at 24 hpf showed a significant increase in the number of double-positive HSPCs in the AGM from 30 to 46 hpf (Fig. 2c, d). Single-cell analysis showed that this change is mainly due to a significant increase in the frequency of HSPCs directly specified from the haemogenic endothelium, while no increase in the rate of cell division or AGM retention was observed (Extended Data Fig. 2). The additional HSPCs produced after 11,12-EET treatment successfully homed to their next niche, resulting in increased numbers of HSPCs in the CHT, which was verified by *in situ* hybridization for the HSPC marker *cmyb* (Fig. 2e and Extended Data Fig. 3). Time-lapse imaging of Tg(*Runx1+23:GFP*) zebrafish showed that 11,12-EET treatment between 24 and 48 hpf increased the rate of arrival of GFP$^+$ HSPCs to the CHT (Fig. 2f and Supplementary Videos 1 and 2), presumably owing to enhanced HSPC specification in the AGM.

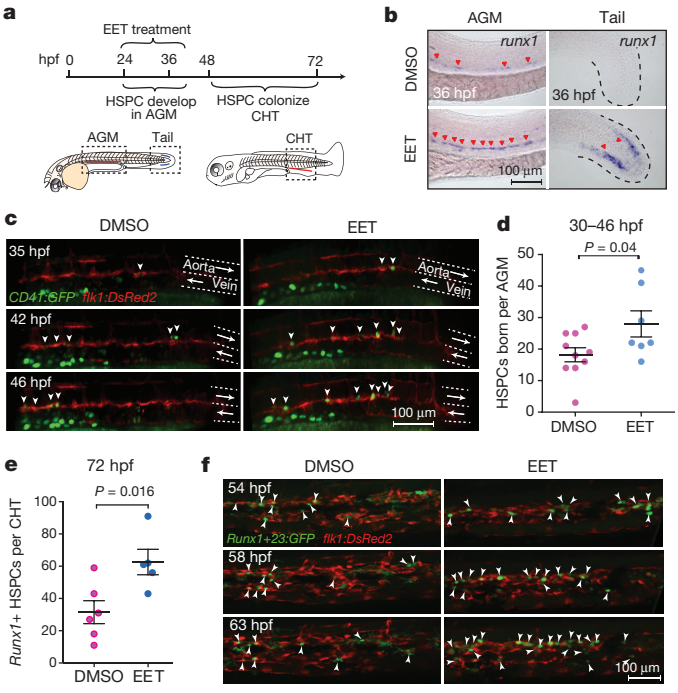

Figure 2 | 11,12-EET enhances HSPC specification in the zebrafish embryo AGM. **a**, Schematic of HSPC development in zebrafish embryos. **b**, Representative images of whole-mount *in situ* hybridization showing 11,12-EET (24–36 hpf treatment) induced HSPC marker *runx1* in the AGM and a tail non-haematopoietic tissue (>8 independent experiments, $n > 100$). **c**, **d**, 11,12-EET (24–46 hpf) enhanced *CD41:GFP/flk1:DsRed2* double-positive HSPCs (white arrowheads) emerging in the AGM. Arrows indicate blood flow. **e**, **f**, Same treatment increased the number of HSPCs in the CHT. **e**, mCherry$^+$ HSPCs quantified in the Tg(*Runx1+23:mCherry*) CHT. **f**, Representative montage images of *Runx1+23:GFP* HSPCs (white arrowheads) engrafting CHT. *flk1:DsRed2*, endothelial cells. Unpaired two-tailed *t*-test, mean and s.e.m. (**d**, **e**).

To dissect the molecular mechanism leading to *runx1* induction further, we performed microarray analysis on 11,12-EET-treated 36-hpf embryos (Supplementary Table 3). The upregulation of multiple activator protein 1 (AP-1) family transcription factors, including *fosl2*, and duplicated orthologues of human JUNB, *junb* and *junbl*, were among the most prominent changes. Whole-mount *in situ* hybridization confirmed the induction both in the AGM and the non-haematopoietic region of the tail mesenchyme (Fig. 3d, top two rows). AP-1 messenger RNA transcripts were detectable within 1 h of 11,12-EET treatment and insensitive to the protein translation inhibitor cycloheximide (Extended Data Fig. 4a, b), indicating that AP-1 members are immediate targets of EET signalling. By contrast, *runx1* induction required at least 4 h of 11,12-EET treatment and was completely blocked by cycloheximide (Extended Data Fig. 4c). Therefore, we proposed that EET-induced AP-1 expression is necessary for increasing *runx1* transcription.

To test this hypothesis genetically, we globally knocked down AP-1 with anti-sense morpholinos targeting *junb* and *junbl*, which blocked *runx1* expression without affecting endothelial cells of the AGM (Extended Data Fig. 5), suggesting that AP-1 might be required for HSPC specification from haemogenic endothelium. To test whether *AP-1* function is autonomous to the haemogenic endothelium, we delivered a dominant-negative form of JunB protein (dnJUNB) specifically to the *flk1*+ endothelial cells, before the induction of *runx1*, to functionally inhibit all AP-1 activity. Although *flk1:dnJUNB* did not significantly reduce the expression of *runx1* in DMSO-treated embryos, it suppressed the EET-induced increase of *runx1* in the AGM (Fig. 3a, b). Combined with the gene expression data, these genetic analyses showed that 11,12-EET activates an AP-1 and *runx1* transcriptional cascade of cell-fate specification autonomous to the haemogenic endothelium.

In an effort to define downstream signalling events for 11,12-EET, we performed a chemical suppressor screen in zebrafish embryos by examining the capability of various chemicals to suppress the 11,12-EET-induced AP-1 and *runx1* gene signature (Fig. 3c). Several PI(3)K inhibitors completely blocked the signature without detrimental effects to overall embryonic development (Fig. 3d, e and Extended Data Fig. 6a). To interrogate specific PI(3)K catalytic subunits, we assayed subunit-specific chemical inhibitors and morpholinos targeting individual class I PI(3)K subunits. Among α-, β-, γ- and δ-subunits of PI(3)K, only PI(3)Kγ loss of function specifically abrogated the *runx1* induction in the AGM and tail non-haematopoietic tissue (Extended Data Fig. 6b, c). Furthermore, 11,12-EET enhanced PI(3)K activity in immortalized human umbilical vein endothelial cells, assayed by Akt phosphorylation (data not shown). No such increase was seen in human umbilical cord blood CD34$^+$ HSPCs, although EET-induced gene expression changes could be partially blocked in these cells by co-treatment with PI(3)K inhibitors. This indicates PI(3)K functions either directly downstream of 11,12-EET or as a parallel pathway, depending on the cellular context. In either case, PI(3)K activity is required for inducing the AP-1 and *runx1* transcription cascade in the AGM.

To understand how 11,12-EET treatment leads to increased engraftment in already-specified HSPCs, we performed RNA-sequencing in human umbilical cord blood CD34$^+$ HSPCs and a human myeloid cell line (U937), and used Ingenuity Pathway Analysis (IPA) to decipher the biological pathways regulated by 11,12-EET in both cell types

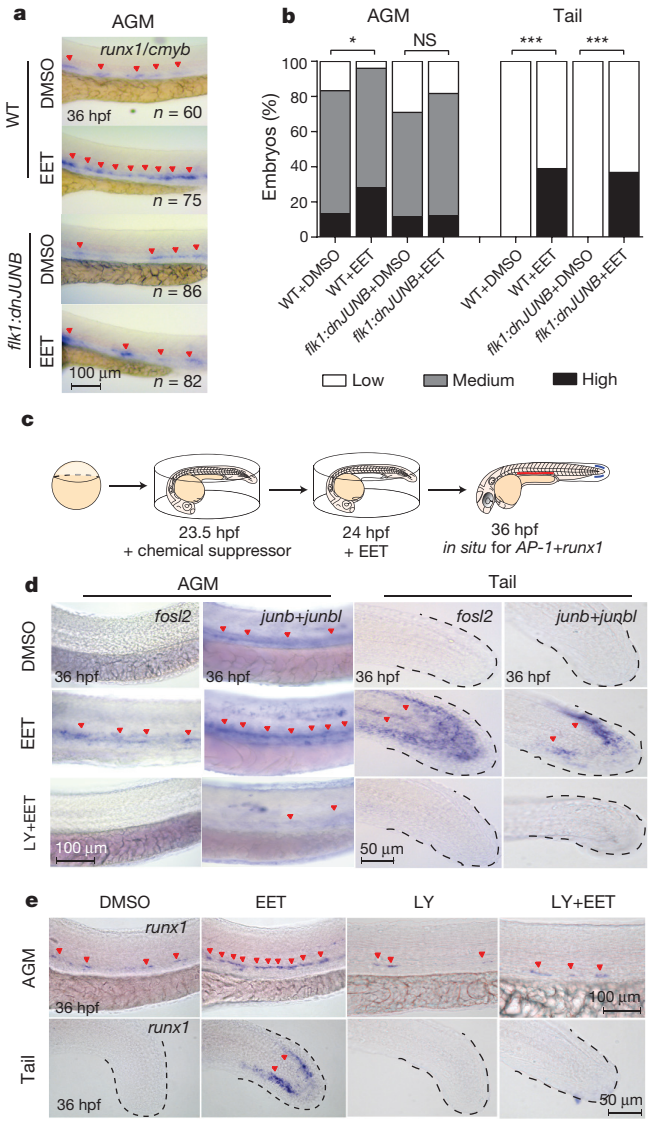

Figure 3 | 11,12-EET induces a PI(3)K-dependent AP-1/*runx1* transcriptional program to increase HSPC specification. **a**, **b**, Stable *flk1:dnJUNB-2A-GFP* expression blocking AP-1 function suppressed 11,12-EET-enhanced HSPCs in the AGM. Representative images of *runx1* and *cmyb in situ* hybridization (**a**) and quantification (**b**) after 11,12-EET treatment (24–36 hpf). Embryos scored as high, medium or low *runx1* and *cmyb*, summed across 4 experiments. $*P = 0.01$, $***P < 0.0001$, Chi-square. NS, not significant; WT, wild-type. **c**, Schematic of chemical screen for EET signalling pathway suppressors. **d**, **e**, 11,12-EET induced AP-1 family transcription factors (*fosl2*, *junb* and *junbl*) (**d**) and *runx1* (**e**), suppressed by cotreatment with the PI(3)K inhibitor LY294002 (LY), in the AGM and tail (**d**, **e**) (three independent experiments, $n > 40$). Same images from Fig. 2b were used as staining controls (**e**).

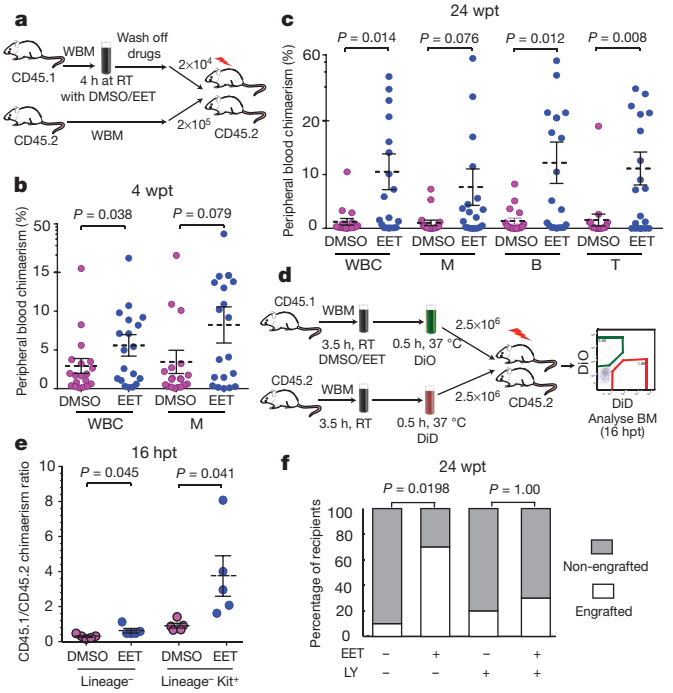

Figure 4 | 11,12-EET enhances HSPC engraftment and homing in mammals. **a**, Schematic of mouse WBM competitive transplantation. RT, room temperature. **b**, **c**, Four hours of 11,12-EET treatment promoted short-term WBM engraftment at 4 wpt (**b**) and long-term multilineage engraftment at 24 wpt (**c**). B, B cells; M, myeloid cells; T, T cells; WBC, white blood cells. Two independent experiments combined, $n = 20$ total. **d**, Schematic of WBM competitive homing assay. DiD and DiO denote cell-labelling solutions. **e**, 11,12-EET increased homing efficiency of Lin^- cells and Lin^- Kit^+ HSPCs ($n = 5$). **f**, PI(3)K activation is required for EET-enhanced mouse WBM engraftment ($n = 10$). LY, 10 μM LY294002. Recipients characterized as engrafted or non-engrafted based on peripheral blood WBC chimaerism, two-tailed Fisher's exact test (**b**, **f**); unpaired two-tailed *t*-test (**c**, **e**), mean and s.e.m.

(Extended Data Fig. 7 and Supplementary Table 4). Cell-to-cell signalling and cellular movement networks topped the list of activated biological pathways, including the AP-1 members, which have been shown to modulate cell migration in many cell types[16,17]. AP-1 thus seems to be a common target of EET signalling, which leads to the induction of *runx1* in the haemogenic endothelium (Fig. 3), and probably supports cell migration and cell–cell signalling of already-specified haematopoietic cells. By contrast, *RUNX1* is not upregulated in already-specified HSPCs, which is consistent with previous studies showing that *Runx1* is dispensable for HSPCs to engraft later haematopoeitic sites[18]. Several cytokines, such as *CXCL8*, *OSM* and *CCL2*, were also upregulated and involved in the cell migration network.

These data show that besides promoting HSPC specification from the haemogenic endothelium, 11,12-EET can also directly induce gene expression programs beneficial for engraftment in already-specified HSPCs. Similarly, 11,12-EET treatment of zebrafish embryos after 48 hpf, when AGM HSPC production has already completed, leads to increased HSPCs in the CHT in a PI(3)Kγ-dependent manner, without affecting cell apoptosis or proliferation (Extended Data Fig. 8). Our data strongly suggest that 11,12-EET modulates cell migration and cell–cell interaction during HSPC engraftment.

To test the evolutionary conservation of EET-induced haematopoietic phenotypes, we examined the effect of 11,12-EET on HSPC engraftment in mammalian bone marrow competitive transplantation. Consistently, 11,12-EET promoted greater short-term chimaerism by 4 weeks post-transplant compared to control-treated cells (Fig. 4a, b). Even up to 24 weeks, EET-treated marrow maintained greater multi-lineage contribution (Fig. 4c). Enhanced short- and long-term engraftment suggests that 11,12-EET may affect both stem and progenitor cells, perhaps by establishing a competitive advantage at the early stage of engraftment. In a whole-bone-marrow (WBM) homing assay, we found 11,12-EET promoted the initial seeding of progenitor cells in the bone marrow (Fig. 4d, e). The early effect could be due to an enhanced cell migration and cell–cell signalling program, since assaying cell proliferation or apoptosis in whole marrow immediately after 11,12-EET treatment did not show significant changes (Extended Data Fig. 9). However, this does not exclude the possibility of a later onset of anti-apoptotic effects on transplantation. Finally we found transient inhibition of PI(3)K partially blocked EET-induced enhancement of long-term, multi-lineage engraftment after mouse

bone marrow transplant (Fig. 4f). Thus, the EET effect on enhancing HSPC engraftment is evolutionarily conserved in fish and mammals.

Our unbiased chemical genetic studies establish a new eicosanoid pathway for haematopoiesis, which increases HSPC specification in the AGM by inducing AP-1 and *runx1*, and also enhances HSPC engraftment by modulating several biological pathways, such as migration and cell–cell signalling. Previous work in our laboratory discovered a different eicosanoid, PGE_2, could also enhance marrow engraftment[4,5]. Both PGE_2 and EETs are arachidonic-acid-derived eicosanoids that are locally produced near wounds, and may facilitate progenitor recruitment, engraftment and proliferation. Despite their common origin, the underlying molecular signalling mechanisms and activities of PGE_2 and EETs are different (Supplementary Table 5). Although the direct receptor for EETs is unknown, several studies have provided biochemical evidence that EETs bind to a G-protein-coupled receptor (GPCR)[19,20]. GPCRs signal through various Gα subunits[21]. Previously, we showed that PGE_2 signals through the cAMP-dependent Gαs-coupled PGE_2 receptor for its pro-haematopoietic effects[5]. Using chemical inhibition and genetic loss-of-function approaches, we screened all families of zebrafish Gα subunits. Notably, we found that *gna12* and *gna13* are specifically required for EET-induced AP-1 and *runx1* expression (Extended Data Fig. 10). Inhibiting Gαs did not suppress the EET phenotypes, indicating that EETs and PGE_2 have different signalling mechanisms.

During marrow transplantation, the achieved chimaerism over time is critical, and the time to adequate neutrophil engraftment is an important milestone for treatment success. In addition to improving long-term repopulation, EETs seem to have a prominent effect on progenitor engraftment, as shown by increased chimaerism early after transplantation. Our studies highlight the importance of lipid mediators in regulating HSPC engraftment, and the manipulation of these pathways could have clinical impact for patients undergoing transplantation.

Online Content Methods, along with any additional Extended Data display items and Source Data, are available in the online version of the paper; references unique to these sections appear only in the online paper.

Received 31 October 2012; accepted 11 May 2015.

1. Spector, A. A. & Kim, H.-Y. Y. Cytochrome P450 epoxygenase pathway of polyunsaturated fatty acid metabolism. *Biochim. Biophys. Acta* **1851,** 356–365 (2015).
2. Node, K. *et al.* Anti-inflammatory properties of cytochrome P450 epoxygenase-derived eicosanoids. *Science* **285,** 1276–1279 (1999).
3. White, R. M. *et al.* Transparent adult zebrafish as a tool for *in vivo* transplantation analysis. *Cell Stem Cell* **2,** 183–189 (2008).
4. North, T. E. *et al.* Prostaglandin E2 regulates vertebrate haematopoietic stem cell homeostasis. *Nature* **447,** 1007–1011 (2007).
5. Goessling, W. *et al.* Genetic interaction of PGE2 and Wnt signaling regulates developmental specification of stem cells and regeneration. *Cell* **136,** 1136–1147 (2009).
6. Forsberg, E. C. *et al.* Molecular signatures of quiescent, mobilized and leukemia-initiating hematopoietic stem cells. *PLoS ONE* **5,** e8785 (2010).
7. Panigrahy, D., Greene, E. R., Pozzi, A., Wang, D. W. & Zeldin, D. C. EET signaling in cancer. *Cancer Metastasis Rev.* **30,** 525–540 (2011).
8. Pfister, S. L., Gauthier, K. M. & Campbell, W. B. Vascular pharmacology of epoxyeicosatrienoic acids. *Adv. Pharmacol.* **60,** 27–59 (2010).
9. Wang, Y. *et al.* Arachidonic acid epoxygenase metabolites stimulate endothelial cell growth and angiogenesis via mitogen-activated protein kinase and phosphatidylinositol 3-kinase/Akt signaling pathways. *J. Pharmacol. Exp. Ther.* **314,** 522–532 (2005).
10. Lam, E. Y., Hall, C. J., Crosier, P. S., Crosier, K. E. & Flores, M. V. Live imaging of Runx1 expression in the dorsal aorta tracks the emergence of blood progenitors from endothelial cells. *Blood* **116,** 909–914 (2010).
11. Bertrand, J. Y. *et al.* Haematopoietic stem cells derive directly from aortic endothelium during development. *Nature* **464,** 108–111 (2010).
12. Kissa, K. & Herbomel, P. Blood stem cells emerge from aortic endothelium by a novel type of cell transition. *Nature* **464,** 112–115 (2010).
13. Boisset, J. C. *et al. In vivo* imaging of haematopoietic cells emerging from the mouse aortic endothelium. *Nature* **464,** 116–120 (2010).
14. Murayama, E. *et al.* Tracing hematopoietic precursor migration to successive hematopoietic organs during zebrafish development. *Immunity* **25,** 963–975 (2006).
15. Tamplin, O. J. *et al.* Hematopoietic stem cell arrival triggers dynamic remodeling of the perivascular niche. *Cell* **160,** 241–252 (2015).
16. Renaud, S. J., Kubota, K., Rumi, M. A. & Soares, M. J. The FOS transcription factor family differentially controls trophoblast migration and invasion. *J. Biol. Chem.* **289,** 5025–5039 (2014).
17. Gilan, O. *et al.* PR55α-containing protein phosphatase 2A complexes promote cancer cell migration and invasion through regulation of AP-1 transcriptional activity. *Oncogene* **34,** 1333–1339 (2015).
18. Chen, M. J., Yokomizo, T., Zeigler, B. M., Dzierzak, E. & Speck, N. A. Runx1 is required for the endothelial to haematopoietic cell transition but not thereafter. *Nature* **457,** 887–891 (2009).
19. Chen, Y., Falck, J. R., Manthati, V. L., Jat, J. L. & Campbell, W. B. 20-Iodo-14,15-epoxyeicosa-8(Z)-enoyl-3-azidophenylsulfonamide: photoaffinity labeling of a 14,15-epoxyeicosatrienoic acid receptor. *Biochemistry* **50,** 3840–3848 (2011).
20. Yang, W. *et al.* Characterization of epoxyeicosatrienoic acid binding site in U937 membranes using a novel radiolabeled agonist, 20–125i-14,15-epoxyeicosa-8(Z)-enoic acid. *J. Pharmacol. Exp. Ther.* **324,** 1019–1027 (2008).
21. Lappano, R. & Maggiolini, M. G protein-coupled receptors: novel targets for drug discovery in cancer. *Nature Rev. Drug Discov.* **10,** 47–60 (2011).
22. Frömel, T. *et al.* Soluble epoxide hydrolase regulates hematopoietic progenitor cell function via generation of fatty acid diols. *Proc. Natl Acad. Sci. USA* **109,** 9995–10000 (2012).

Supplementary Information is available in the online version of the paper.

Acknowledgements We thank C. R. Lee, M. L. Edin and N. Gray for providing reagents; Y. Zhou, A. Dibiase, S. Yang, S. Datta, P. Manos, R. Mathieu and M. Ammerman for technical assistance; H. Huang for providing graphic illustration; R. M. White, T. E. North and C. Mosimann for discussion. Microarray studies were performed by the Molecular Genetics Core Facility at Boston Children's Hospital, supported by NIH-P50-NS40828 and NIH-P30-HD18655. S. Li in Y. Zhang's laboratory at the Longwood HHMI joint core facility helped with RNA-seq. L.I.Z. and G.Q.D. are Howard Hughes Medical Institute (HHMI) investigators. This work was supported by HHMI and National Institutes of Health (NIH) grants R01 HL04880, P015PO1HL32262-32, 5P30 DK49216, 5R01 DK53298, 5U01 HL10001-05, R24 DK092760, and 1R01HL097794-04 (to L.I.Z.). This work was also funded, in part, by the Intramural Research Program of the NIH, National Institute of Environmental Health Sciences (Z01 ES025034 to D.C.Z.), the National Cancer Institute grant ROCA148633-01A5 (D.P.), and DFG and Care-for-Rare Foundation (V.B.).

Author Contributions P.L. and L.I.Z. designed the study, analysed data and wrote the manuscript, with help from J.L.L. and V.B. P.L. developed the zebrafish competitive transplantation and performed the chemical screen with technical help from E.K.P. P.L. performed the mouse experiments with technical help from T.V.B., S.M. and G.C.H. P.L. performed the zebrafish microarray and embryo chemical/genetic suppressor screens with technical help from E.B.R. J.L.L. performed zebrafish embryo genetic studies and AGM timelapse imaging. V.B. performed RNA-seq and analysis on human cells with technical help from F.G.B. O.J.T. performed CHT time-lapse imaging. T.M.S. provided the chemical library. D.P. and D.C.Z. offered reagents and information related to the EET study. All authors discussed the results and commented on the manuscript.

Author Information The gene expression profiling data have been deposited in the Gene Expression Omnibus (GEO) under the accession code GSE66767. Reprints and permissions information is available at www.nature.com/reprints. The authors declare competing financial interests: details are available in the online version of the paper. Readers are welcome to comment on the online version of the paper. Correspondence and requests for materials should be addressed to L.I.Z. (zon@enders.tch.harvard.edu).

METHODS

Zebrafish strains. Zebrafish were maintained in accordance with Animal Research Guidelines at Boston Children's Hospital (BCH). The following transgenic zebrafish were used in this study: Tg(*β-actin:GFP*)[23], *casper*[3], RedGlo (ubiquitous *DsRed2* transgenic)[24], Tg(*flk1:DsRed2*)[25], Tg(*CD41:GFP*)[26], Tg(*Runx1+23:mCherry*)[15] and Tg(*Runx1+23:GFP*)[15]. The +23 enhancer region of mouse *Runx1* was used to drive HSPC-specific expression[27]. Tg(*flk1:dnJUNB-2A-GFP*) was constructed by cloning a human JUNBΔN into a *tol2* transgenesis vector[28].

Chemical treatment. The ICCB Known Bioactive Library was purchased from BIOMOL (Enzo Life Sciences) and used for the adult zebrafish transplantation-based chemical screen. Chemicals were diluted at a 1:200 ratio. Chemicals used for the secondary round of screening for confirmation were from a different aliquot of the library, independent of the primary screen plate. 11,12-EET (Cayman Chemical, 50511) was resuspended in DMSO with original organic solvent evaporated. AS605240 (Sigma-Aldrich A0233) was resuspended in DMSO. The following chemicals were used for zebrafish marrow treatment: $dmPGE_2$ (Cayman, 14750), 10 μM; BIO (EMD), 0.5 μM. 0.5 μM 11,12-EET and 14,15-EET were used for zebrafish WKM treatment (Fig. 1e); 2 μM 11,12-EET for all mouse WBM treatment (Fig. 4); and 5 μM 11,12-EET for all zebrafish embryo treatment (Figs 2 and 3). The concentrations were chosen based on dose titration pilot experiments with doses spanning 0.1 to 50 μM. For the chemical suppressor screen, the suppressors were added 30 min before 11,12-EET. Zebrafish embryos were incubated with inhibitors at three different concentrations. The highest effective concentrations tested without causing general toxicity are listed in Supplementary Table 1.

Adult zebrafish kidney marrow transplantation and chemical screen. Adult zebrafish transplantation-based chemical screen was done at the human embronyic stem cell core at BCH. Three-month-old *casper* recipients (both male and female) received split-dose irradiation of 15 Gy each two days and one day before transplantation. Adult zebrafish kidney marrow cells from multiple donors were dissected, pooled together, processed into single-cell suspension and injected retro-orbitally as described previously[29]. Tg(*β-actin:GFP*) WKM cells were incubated with DMSO control or chemicals in 0.9× DPBS plus 5% heat-inactivated FBS for 4 h at room temperature, at a density of 1,000 cells μl^{-1}. Chemicals were washed off before 20,000 treated Tg(*β-actin:GFP*) WKM and 80,000 untreated RedGlo WKM were mixed together and co-injected into irradiated *casper* recipients. The number of recipients per treatment condition in the chemical screen ($n = 10$) was estimated based on preliminary experiments comparing the WKM treated with DMSO or the positive control chemical, $dmPGE_2$. In each experiment, recipients were randomly assigned to each treatment group. All primary hits were cherry-picked and tested in a secondary round of screening ($n = 10$ each). Recipients that died before 4 wpt, mostly owing to infection, were excluded from the analysis. No statistically significant association was observed between recipients' survival rate and a particular drug treatment.

Adult zebrafish fluorescence imaging and quantification. All zebrafish WKM transplantation results shown were obtained at 4 wpt. Transplanted adult *casper* recipients were anaesthetized with 0.2% Tricaine and imaged using a Zeiss Discovery V8 fluorescence stereomicroscope with GFP/RFP filters. To quantify the relative engraftment level in adult zebrafish, the kidney region was manually annotated for each fish, and the average fluorescence intensity of GFP and DsRed2 within the same region was measured (G_{kid} and R_{kid}) using ImageJ. The average background fluorescence intensity (G_{bkg} and R_{bkg}) was measured in a region outside the fish and a mean from multiple images within an experiment was used for all the background subtraction. The relative engraftment level was calculated as $G/R = (G_{kid} - G_{bkg})/(R_{kid} - R_{bkg})$. The investigator analysing the data was blinded to the chemical treatment conditions. For the chemical treatment and screen results (Fig. 1e), the mean G/R in the DMSO group was normalized to 1, and all other groups were normalized to the mean G/R of DMSO. Normalized results from 2–3 independent experiments were pooled for the same chemical.

Zebrafish embryo live imaging. For live imaging, zebrafish embryos were embedded in agarose as described before[11,15]. Single-frame images or time-lapse movies were taken on a spinning disk confocal microscope with an incubation chamber. Images of HSPC birth in the AGM were taken every 10 min. Images of the CHT engraftment process were taken every 2 min. Image post-processing and the creation of the supplementary videos were done with Fluorender, ImageJ, and Imaris.

Zebrafish embryo whole-mount *in situ* hybridization, anti-sense morpholino knockdown and mRNA overexpression. Whole-mount mRNA *in situ* hybridization experiments were performed based on the standard protocol with some modifications (http://zfin.org/zf_info/zfbook/chapt9/9.8.html). Embryos were scored blindly. All of the morpholinos were initially tested at 2, 4 and 6 ng to decide the effective dosage. If the morpholino did not produce a phenotype at 6 ng, additional higher doses were tested (8, 12 ng), until the morpholino caused toxicity. See Supplementary Table 2 for morpholino sequences. *PtxA* (pertussis toxin A, Gαi inhibitor) mRNA (Addgene, plasmid 16678)[30] was *in vitro* transcribed with SP6 RNA polymerase (Ambion, mMESSAGE mMACHINE SP6, AM1340) and injected into one-cell stage zebrafish embryos at 3 pg per embryo, causing morphological defects but no general toxicity.

Zebrafish embryo proliferation and apoptosis assays. Zebrafish embryos were chemically treated between 48 and 72 hpf, and fixed at 72 hpf. For proliferation analysis, embryos were permeablized and stained with primary antibody against phospho-histone H3, and FITC-conjugated secondary antibody. Embryos were imaged and phospho-H3-positive cells in the CHT were manually counted. Secondary antibody-only control showed no nonspecific staining. For apoptosis analysis, embryos were stained using the colorimetric TUNEL staining kit (Promega).

Cell culture. Human $CD34^+$ cells were isolated from fresh umbilical cord blood by Ficoll separation of mononuclear cells and subsequent positive selection of $CD34^+$ cells using magnetic beads (Miltenyi). Cells were treated in serum-free IMDM media (Sigma-Aldrich) with either DMSO or 5 μM 11,12-EET for 2 h at 37 °C. U937 cells[31] were cultured in RPMI-1640 Medium (Sigma-Aldrich) and 10% FBS at 5% CO_2 in air atmosphere according to the protocol (purchased from ATCC without additional confirmation or examination for mycoplasma contamination). For *in vitro* treatment, cells were serum-starved for 1 h and then treated with either DMSO or 5 μM 11,12-EET for 2 h at 37 °C. The conditions for use of human umbilical cord blood $CD34^+$ cells are governed by the associated institution's Internal Review Board (IRB) on behalf of the DF/HCC in accordance with Department of Health and Human Services regulations at 45 CFR Part 46. Informed consent was obtained from all subjects.

Mouse bone marrow transplant. All mice were maintained according to IACUC approved protocols in accordance with BCH animal research guidelines. Nine-week-old CD45.1 and CD45.2 (C57/BL6) male mice were purchased from Jackson Laboratories and housed for 2–3 weeks before the experiments. All CD45.2 recipients received an 11 Gy split dose of γ-irradiation before transplantation, and were randomly assigned to each treatment group. 20,000 CD45.1 WBM cells from age- and gender-matched BL6 donors were treated in DMEM plus 2% FBS at room temperature for 4 h with 2 μM 11,12-EET. For the suppressor experiment (Fig. 4f), 10 μM LY294002 was added to the cells 30 min before the addition of 11,12-EET. Chemicals were washed off before cells were resuspended in PBS and mixed with 200,000 fresh CD45.2 mouse WBM cells. Donor cells were retro-orbitally injected into CD45.2 recipients. Each treatment condition included 10 recipients per experiment. The 12-week survival rate in each experiment was 90–95%, and recipients that died before 12 wpt were excluded from the analysis.

Mouse peripheral blood chimaerism analysis. Peripheral blood was stained with lineage-specific antibodies and analysed on LSRII (BD Biosciences) to assess engraftment. The following antibodies were used: Gr1 (RB6-8C5), Mac1 (M1/70), B220 (RA3-B2), CD3 (145-2C11) and Ter119 from eBioscience; CD45.1 and CD45.2 from BD Biosciences. The CD45.1 chimaerisms in non-irradiated, untransplanted CD45.2 mice were used as a negative staining control. Recipients with multi-lineage chimaerism above the average negative-control chimaerism plus 3 standard deviations were considered to have multi-lineage engraftment (Fig. 4f).

Mouse competitive homing assay. The mouse competitive homing experiment was performed as described, with modifications[32]. In brief, CD45.1 mouse WBM were treated with either DMSO or 2 μM 11,12-EET at room temperature for 3.5 h at a density of 2×10^6 cells per ml. DiO dye was added to the cell suspension (1:200) and incubated at 37 °C for 30 min. At the same time, WBM from CD45.2 mice were incubated at room temperature for 3.5 h without chemical treatment, then labelled with DiD dye (1:200) at 37 °C for 30 min. After the incubation and labelling, the chemicals and dyes were washed off. The DiO-labelled CD45.1 bone marrow and DiD-labelled CD45.2 WBM were mixed at a 1:1 ratio and competitively transplanted into CD45.2 recipients (2.5×10^6 from each donor). Recipients received total body irradiation of 11 Gy one day before transplantation. 16 h after transplant, the recipients were euthanized and bone marrow was analysed by flow cytometry for both DiO/DiD and surface lineage markers (Gr1, Mac1, B220, CD3, Ter119, from Ebioscience) and c-Kit (2B8, BD Biosciences). The ratio between the percentages of DiO^+ (donor) and DiD^+ (competitor) cells within different cell populations was quantified. DiO and DiD are from Vybrant Multicolor Cell-Labelling Kit (Molecular Probes, V-22889).

Mouse bone marrow apoptosis and proliferation assays. For apoptosis analysis, mouse WBM cells were treated with DMSO or 2 μM 11,12-EET for 4 h *in vitro* and stained using the AnnexinV apoptosis kit (BD Biosciences), together with antibodies against lineage markers, Sca-1 (E13-161.7) and c-Kit (2B8). The 7-AAD^-/annexinV^+ cells are the apoptotic population. For proliferation analysis, mouse WBM were treated with DMSO or 2 μM 11,12-EET for 4 h *in vitro*, in the presence

of 10 μM BrdU, then fixed, permeabilized and stained with anti-BrdU antibody (BD Pharmingen BrdU Flow Kits)[33], together with antibodies against lineage markers, Sca-1 and c-Kit.

Gene expression profiling and IPA analysis. Gene expression profiling data are available in GEO (accession numbers GSE39707 and GSE66767). For the zebrafish embryo gene expression study, total RNA was extracted from 36 hpf zebrafish embryos treated with DMSO or 5 μM 11,12-EET between 24 and 36 hpf, with three biological replicates each and $n = 25$ in each group. Microarray hybridization was performed with the Affymetrix GeneChip Zebrafish Genome Array. Hybridized microarray was background-corrected, normalized and multiple-tested using Goldenspike (http://www2.ccr.buffalo.edu/halfon/spike/) in R/Bioconductor[34]. Genes with $q < 0.1$ by SNR test were considered differentially expressed (Supplementary Table 3). For RNaseq analysis on human cells, total RNA was extracted from treated $CD34^+$ and U937 cells with the RNeasy mini plus kit from Qiagen. After quality control on the Bioanalyzer (Agilent), total RNA was depleted of ribosomal RNA with the RiboZero gold kit (Epicentre). Enriched mRNA was applied to library preparation according to manufacturer's protocol (NEBNext Ultra). After repeated quality control for average DNA input size of 300 base pairs (bp), samples were sequenced on a HiSeq Illumina sequencer with 2×100-bp paired-end reads. Quality control of RNA-Seq data sets was performed by FastQC (http://www.bioinformatics.babraham.ac.uk/projects/fastqc/) and Cutadapt[35] to remove adaptor sequences and low quality regions. The high-quality reads were aligned to UCSC build hg19 of the human genome using Tophat 2.0.11 without novel splicing form calls[36]. Transcript abundance and differential expression were calculated with Cufflinks 2.2.1 (ref. 37). FPKM values were used to normalize and quantify each transcript. $\log_2$(fc) ($\log_2$ fold change), P and q values were calculated. As the experiment was not performed in biological replicates, the P and q values were not taken into consideration for further analysis of the data. Results are listed with a cutoff of $\log_2(\text{fc}) > 0.5$ for upregulated genes and $\log_2(\text{fc}) < -0.5$ for downregulated genes in Supplementary Table 4. Analysis of overlapping upregulated genes in both cell types after EET treatment was done using Venny (http://bioinfogp.cnb.csic.es/tools/venny/index.html). The list of overlapping genes was analysed using IPA (QIAGEN) to map enriched bio-functions.

Statistics. The comparison of multi-lineage engraftment in Fig. 4b and f were done by two-tailed Fisher's exact test by comparing the number of engrafted versus non-engrafted recipients. Using the mean chimaerism plus 2× s.e.m. in the DMSO control group as the cutoff, recipients with a chimaerism higher than the cutoff were considered engrafted (Fig. 4b). Embryos in the *in situ* hybridization experiments were scored blindly and analysed by Chi-square tests or two-tailed Fisher's exact test in the case of small sample sizes. The rest of the statistics were done with unpaired two-tailed t-test. Graphs show mean with s.e.m. No statistical methods were used to predetermine sample size. All the zebrafish embryos, adult zebrafish and mice for transplantation were randomized into each treatment group.

23. Traver, D. *et al.* Transplantation and *in vivo* imaging of multilineage engraftment in zebrafish bloodless mutants. *Nature Immunol.* **4,** 1238–1246 (2003).
24. Blake, A., Crockett, R., Essner, J., Hackett, P. & Nasevicius, A. Recombinant constructs and transgenic fluorescent ornamental fish therefrom. US patent US7,700,825 B2 (2010).
25. Kikuchi, K. *et al.* Retinoic acid production by endocardium and epicardium is an injury response essential for zebrafish heart regeneration. *Dev. Cell* **20,** 397–404 (2011).
26. Ma, D., Zhang, J., Lin, H. F., Italiano, J. & Handin, R. I. The identification and characterization of zebrafish hematopoietic stem cells. *Blood* **118,** 289–297 (2011).
27. Bee, T. *et al.* The mouse *Runx1 +23* hematopoietic stem cell enhancer confers hematopoietic specificity to both *Runx1* promoters. *Blood* **113,** 5121–5124 (2009).
28. Ikebe, D., Wang, B., Suzuki, H. & Kato, M. Suppression of keratinocyte stratification by a dominant negative JunB mutant without blocking cell proliferation. *Genes Cells* **12,** 197–207 (2007).
29. Pugach, E. K., Li, P., White, R. & Zon, L. Retro-orbital injection in adult zebrafish. *J. Vis. Exp.* **34,** 1645 (2009).
30. Slusarski, D. C., Corces, V. G. & Moon, R. T. Interaction of Wnt and a Frizzled homologue triggers G-protein-linked phosphatidylinositol signalling. *Nature* **390,** 410–413 (1997).
31. Sundstrom, C. & Nilsson, K. Establishment and characterization of a human histiocytic lymphoma cell line (U-937). *Int. J. Cancer* **17,** 565–577 (1976).
32. Lam, B. S., Cunningham, C. & Adams, G. B. Pharmacologic modulation of the calcium-sensing receptor enhances hematopoietic stem cell lodgment in the adult bone marrow. *Blood* **117,** 1167–1175 (2011).
33. Challen, G. A., Boles, N., Lin, K. K. & Goodell, M. A. Mouse hematopoietic stem cell identification and analysis. *Cytometry A* **75,** 14–24 (2009).
34. Choe, S. E., Boutros, M., Michelson, A. M., Church, G. M. & Halfon, M. S. Preferred analysis methods for Affymetrix GeneChips revealed by a wholly defined control dataset. *Genome Biol.* **6,** R16 (2005).
35. Martin, M. Cutadapt removes adapter sequences from high-throughput sequencing reads. *EMBnet J.* **17,** 1 (2011).
36. Trapnell, C., Pachter, L. & Salzberg, S. L. TopHat: discovering splice junctions with RNA-Seq. *Bioinformatics* **25,** 1105–1111 (2009).
37. Trapnell, C. *et al.* Transcript assembly and quantification by RNA-Seq reveals unannotated transcripts and isoform switching during cell differentiation. *Nature Biotechnol.* **28,** 511–515 (2010).
38. Lee, C. R. *et al.* Endothelial expression of human cytochrome P450 epoxygenases lowers blood pressure and attenuates hypertension-induced renal injury in mice. *FASEB J.* **24,** 3770–3781 (2010).

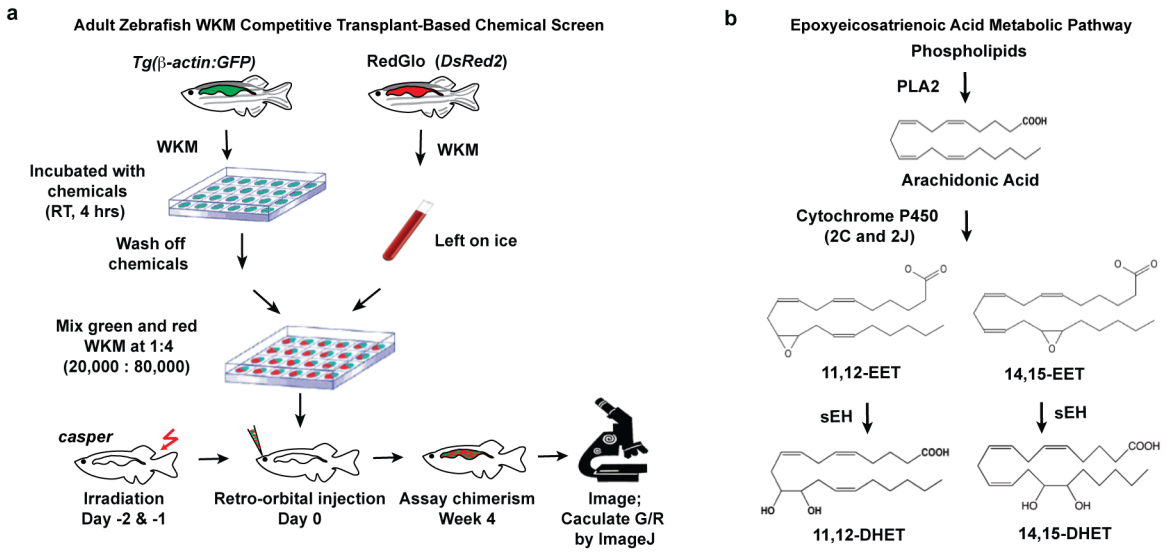

Extended Data Figure 1 | Zebrafish WKM competitive transplantation-based chemical screen identifies EETs as enhancers of marrow engraftment. **a**, WKM from Tg(*β-actin:GFP*) donors were dissected, dissociated as single-cell suspension, and incubated with chemicals at room temperature for 4 h in a round-bottom 96-well plate. Meanwhile, WKM were dissected from RedGlo zebrafish, counted and kept on ice. After the drug treatment, chemicals were washed off and cells were resuspended in 0.9× PBS plus 5% FBS. Approximately 20,000 treated green WKM and 80,000 untreated red WKM were co-injected retro-orbitally into sublethally irradiated *casper* zebrafish ($n = 10$ per chemical). For every independent screening day, negative control (DMSO) and positive control (10 μM $dmPGE_2$) treatments were used for normalization and quality assurance. The engraftment was measured at 4 wpt by fluorescence imaging and ImageJ quantification as described in Fig. 1b. **b**, EET metabolic pathway: arachidonic acid is released by phospholipase A_2 (PLA_2) from the membrane lipid bilayer. EETs are synthesized directly from arachidonic acid by the cytochrome P450 family of epoxygenases, especially 2C and 2J in human[38], and get degraded by soluble epoxide hydrolase (sEH), generating dihydroxyeicosatrienoic acids (DiHET). Four isomers of EET exist *in vivo*: 5,6-, 8,9-, 11,12- and 14,15-EET.

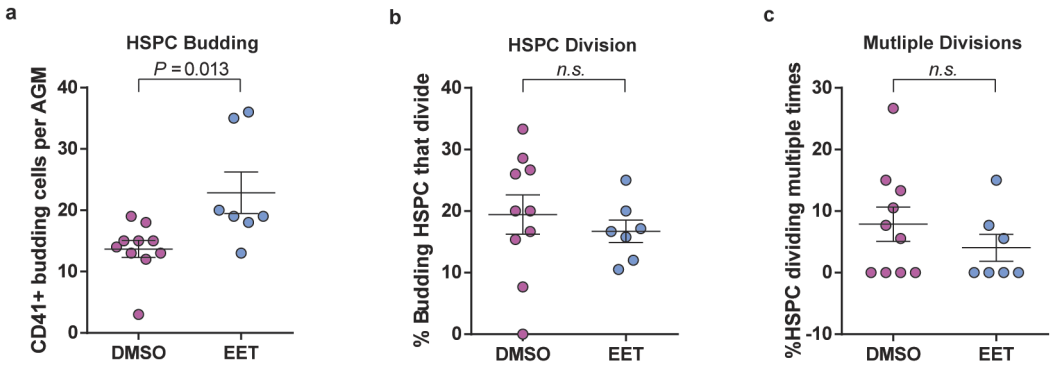

Extended Data Figure 2 | 11,12-EET enhances HSPC specification in the AGM in zebrafish embryos. Tg(*CD41:GFP/flk1:DsRed2*) embryos were treated with DMSO or 5 μM 11,12-EET starting at 24 hpf, then mounted for spinning disc confocal timelapse imaging from 30–46 hpf in the presence of the chemicals. Data are mean and s.e.m., unpaired two-tailed *t*-tests, $n = 10$ for DMSO, $n = 7$ for EET. **a**, More HSPCs are directly specified in EET-treated AGM. Graph shows HSPCs born by direct specification/budding only, excluding cells born by division of an already-budding cell. **b**, **c**, 11,12-EET does not influence the rate of HSPC division in the AGM, shown by per movie, percentage of budding HSPCs that divide at least once (**b**) and divide twice or more (**c**) before leaving the AGM or before the end of timelapse recording.

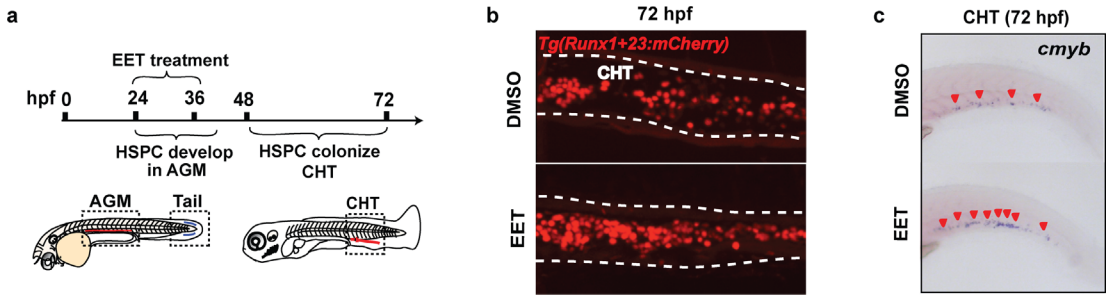

Extended Data Figure 3 | 11,12-EET treatment between 24 and 48 hpf increases the number of HSPCs in the CHT. **a**, Embryos were treated between 24 and 48 hpf with either DMSO or 5 μM 11,12-EET. Chemicals were washed off at 48 hpf, and embryos grew in drug-free environment for another 24 h. **b**, 11,12-EET treatment increased the number of mCherry^{+} HSPCs in the CHT in Tg(*Runx1+23:mCherry*) embryos (see also Fig. 2e). Representative images of the CHT from the two groups. **c**, The same chemical treatment increased the staining of *cmyb*, a HSPC marker, by whole-mount RNA *in situ* hybridization. Representative images from each group (a total of $n > 60$ from three independent experiments).

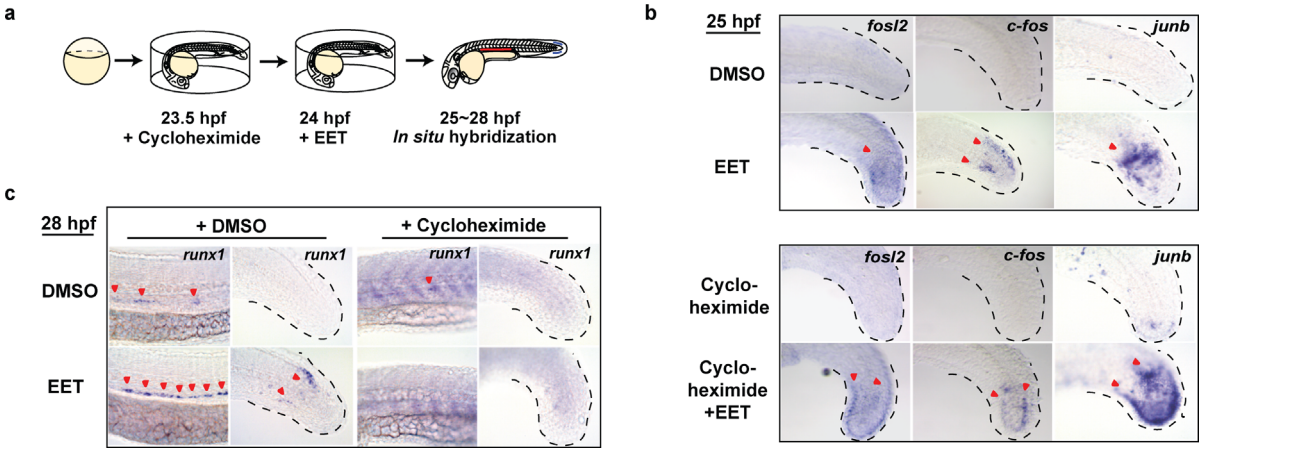

Extended Data Figure 4 | EET signalling pathway activates AP-1 family members as primary transcriptional targets, and *runx1* as a secondary transcriptional target. **a**, Wild-type embryos were incubated with 300 μM cycloheximide, a translation blocker, for 30 min before the addition of 5 μM 11,12-EET at 24 hpf. Embryos were fixed for *in situ* hybridization at 25 hpf or 28 hpf. **b**, AP-1 transcription was induced after 1 h treatment with 11,12-EET, insensitive to cycloheximide inhibition. This means AP-1 induction does not depend on *de novo* protein synthesis, indicating AP-1 members are primary transcriptional targets of the EET signalling pathway. **c**, *runx1* transcription was induced after 4 h treatment with EET (two columns on the left) and cycloheximide completely blocked EET-induced *runx1* expression (two columns on the right). This suggests *runx1* transcription depends on *de novo* protein synthesis of an upstream factor(s) upon EET stimulation, indicating that *runx1* is a secondary transcriptional target of the EET signalling pathway. Representative images from each group (a total of $n > 30$ from two independent experiments).

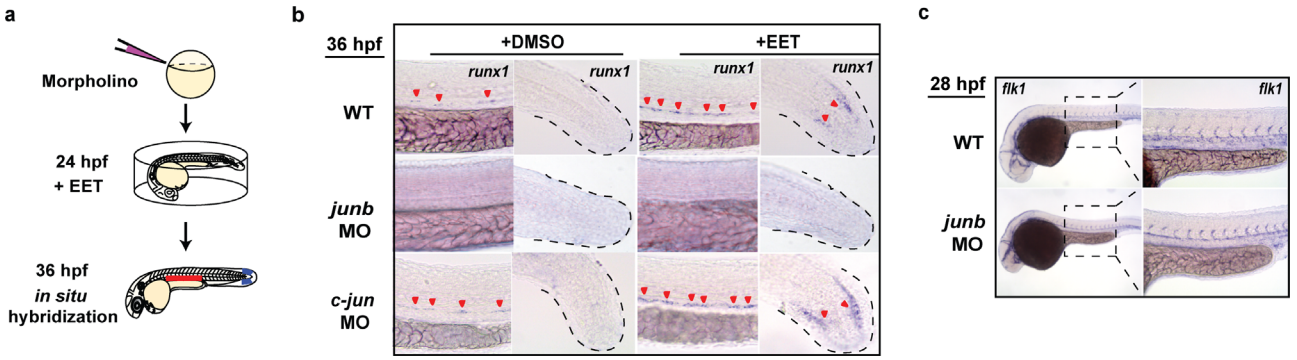

Extended Data Figure 5 | Knocking down *junb* and *junbl* inhibits HSPC specification in the AGM. **a**, Wild-type embryos were injected with antisense morpholinos at the one-cell stage, and treated with DMSO or 5 μM 11,12-EET starting from 24 hpf. Embryos were fixed at 36 hpf for *in situ* hybridization of *runx1*. **b**, Knocking down *junb* completely blocked *runx1* expression at 36 hpf both in the AGM and the tail non-haematopoietic tissue (middle row). By contrast, knocking down *c-jun* did not block the increase of *runx1* (bottom row), consistent with the lack of *c-jun* upregulation in EET-treated embryos (data not shown). **c**, *junb* morphants still developed normal vascular structure in the AGM at 28 hpf, as shown by endothelial marker *flk1*. Representative images from each group (a total of $n > 40$ from three independent experiments).

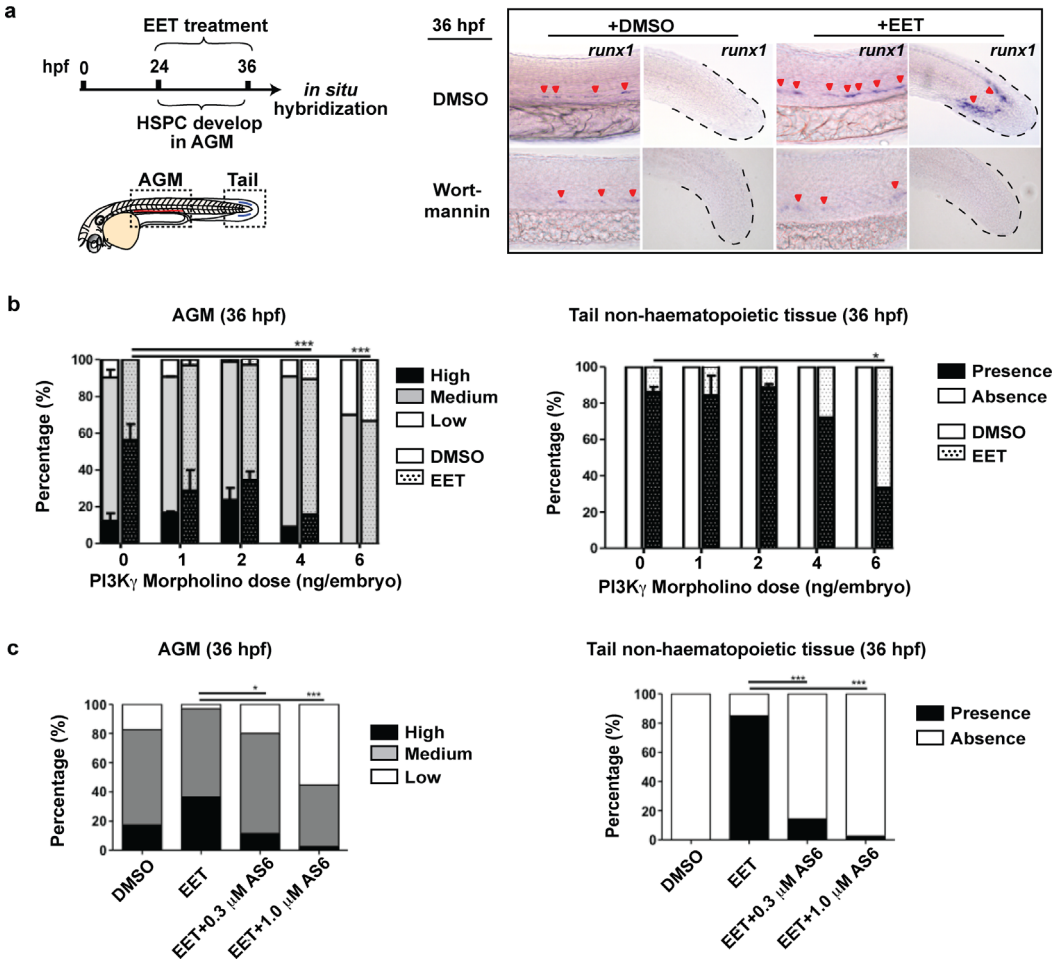

Extended Data Figure 6 | PI(3)Kγ activation is specifically required for EET-induced gene expression signature. **a**, Similar to LY294002 (Fig. 3d–e), another pan-PI(3)K/AKT inhibitor, wortmannin (1 μM), blocked EET-induced *runx1* expression both in the AGM and tail. Representative images from each group (a total of $n > 60$ from three independent experiments). **b**, Morpholinos specific to PI(3)Kγ, but not α, β and δ subunits (data not shown), prevented EET-induced *runx1* in the AGM and tail. Embryos were injected at 1–2-cell stage with the indicated amount of morpholino and treated with DMSO or 5 μM 11,12-EET from 24–36 hpf. *In situ* hybridization for *runx1* performed at 36 hpf and percentages of embryos having high, medium or low expression in the AGM and present or absent expression in the tail are shown. Graph summarizes three experiments, $n \geq 10$ embryos for each condition (0, 1 and 2 ng, data are mean and s.e.m.) or one experiment $n \geq 9$ for all conditions (4 and 6 ng). **c**, The PI(3)Kγ-specific inhibitor AS605240 (AS6) recapitulates the morpholino phenotype. Embryos treated from 24 to 36 hpf with DMSO or 5 μM 11,12-EET, with or without 0.3–1.0 μM AS6, then fixed and stained for *runx1* at 36 hpf. DMSO, $n = 23$; EET, $n = 33$; EET+0.3 μM AS6, $n = 35$; EET+1.0 μM AS6, $n = 38$. $^{*}P < 0.05$, $^{***}P < 0.001$, two-tailed Fisher's exact test.

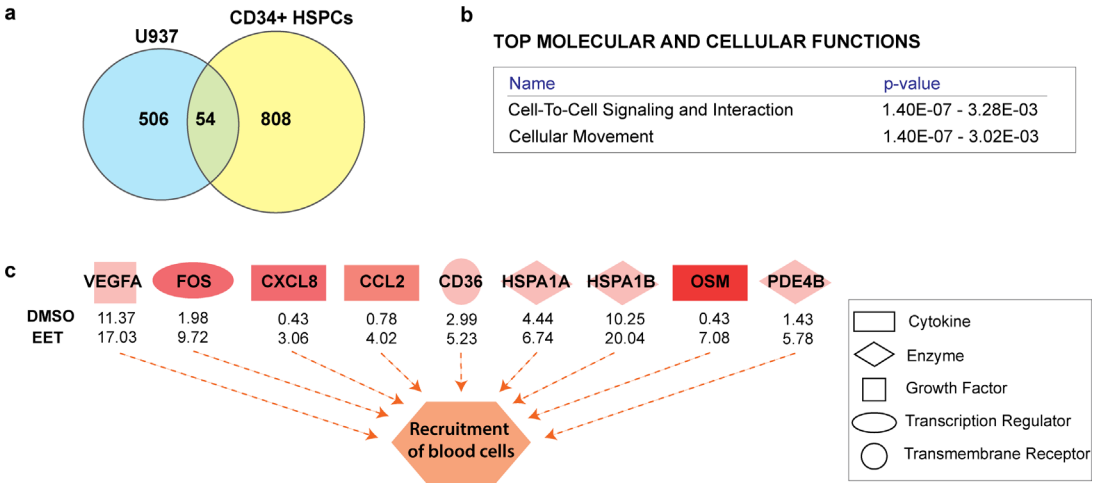

Extended Data Figure 7 | 11,12-EET upregulates genes involved in cell-to-cell signalling and cellular movement in haematopoietic progenitors. **a**, Venn diagram showing a common set of 54 genes upregulated ($\log_2$(fc) > 0.5) after 2 h of 11,12-EET treatment (5 μM), both in human myeloid U937 cells and human umbilical cord $CD34^+$ HSPCs (see also Supplementary Table 4 for lists of up- and downregulated genes). **b**, **c**, Ingenuity Pathway Analysis (IPA) of the overlapping gene set between the two cell types for enrichment of bio-functions. **b**, Biological processes, such as cell-to-cell signalling and cellular movement, were highly enriched, supporting the capability of EETs in enhancing engraftment (see also Supplementary Table 4 for a comprehensive list of all biological functions predicted to be activated or suppressed based on the same gene set). **c**, Activation of recruitment of blood cells is caused by upregulation of chemokines and cytokines such as CXCL8 and OSM after EET treatment, as well as by upregulation of transcription factors, such as AP-1 genes (FOS). Orange dashed arrows depict activation. Shades of red represent the level of activation. Numbers underneath factors show RNaseq FPKM (fragments per kilobase of exon per million reads mapped) values in U937 cells.

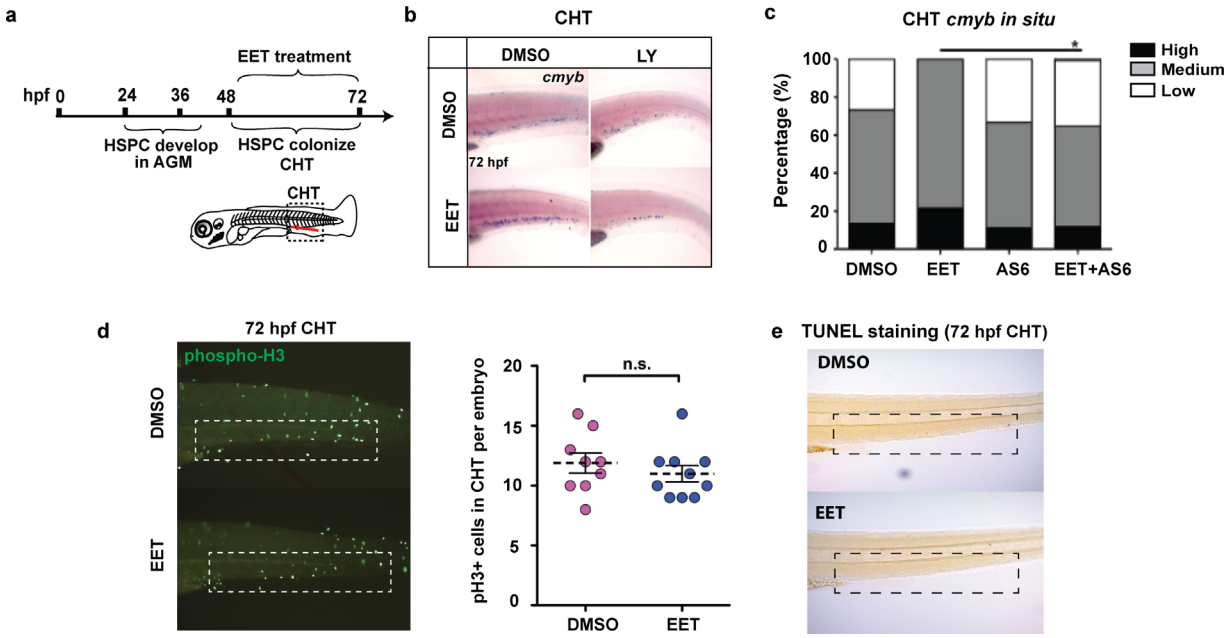

Extended Data Figure 8 | 11,12-EET treatment after HSPC specification still enhances the number of HSPCs in the CHT. **a**, Embryos were treated with DMSO or 5 μM 11,12-EET between 48 and 72 hpf to bypass the HSPC specification process in the AGM. 72-hpf embryos were fixed and tested on the following assays. **b**, *In situ* hybridization for *cmyb*, a marker for HSPCs. EET treatment significantly increased the staining, while LY294002, a pan-PI(3)K inhibitor, suppressed the effect. Representative images from each group (a total of $n > 60$ from four independent experiments). **c**, A PI(3)Kγ-specific inhibitor AS605240 (AS6) also blocked the EET-induced increase of *cmyb* staining. Percentage of embryos having high, medium or low expression in the CHT is shown. $n \geq 11$ for all conditions. Chi-square analysis. **d**, The increase of HSPCs in the CHT is not due to effects on proliferation. Immunofluorescence staining for phospho-histone H3 (pH3) as a marker for proliferating cells. The number of pH3-positive cells was manually counted. Two-tailed *t*-test showed no significant difference between DMSO- versus EET-treated embryos. $n = 9$ for DMSO, $n = 10$ for EET. **e**, TUNEL staining as an assay for apoptotic cells. Apoptosis was minimal in the CHT at 72 hpf. As a staining control, obvious apoptosis was detected in the same embryos in the brain region, and was comparable between DMSO- and EET-treated embryos (data not shown).

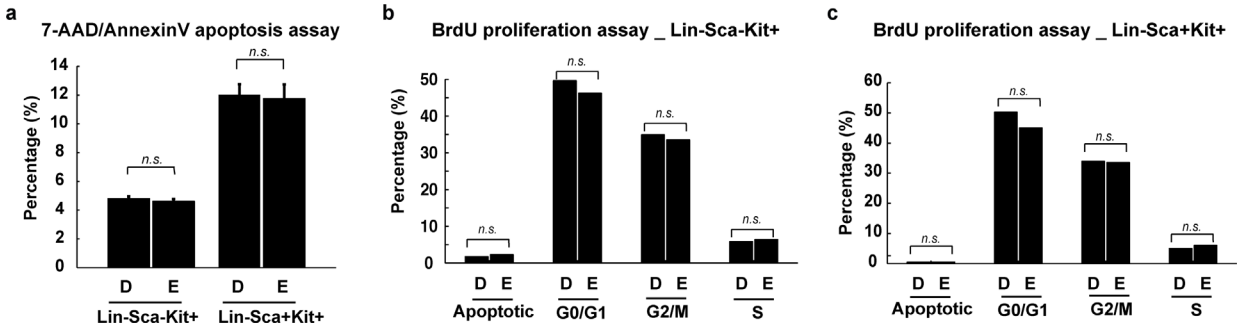

Extended Data Figure 9 | 11,12-EET treatment of mouse WBM does not lead to immediate changes in cell proliferation or apoptosis. **a**, *In vitro* apoptosis assay on WBM treated with DMSO or 2 μM 11,12-EET for 4 h. The 7-AAD-negative and annexinV-positive population are the cells undergoing apoptosis. No significant differences between the two groups were observed either in $Lin^{-}Sca^{-}Kit^{+}$ or $Lin^{-}Sca^{+}Kit^{+}$ progenitor populations ($n = 4$ each), mean and s.e.m. **b**, **c**, *In vitro* proliferation assay on WBM treated with DMSO or 2 μM 11,12-EET for 4 h, in the presence of 10 μM BrdU. No significant differences between the two groups were observed either in $Lin^{-}Sca^{-}Kit^{+}$ (**b**) or $Lin^{-}Sca^{+}Kit^{+}$ populations (**c**) for any cell cycle stage. Unpaired two-tailed *t*-test, $n = 4$ each, bar denotes the mean. D, DMSO; E, EET.

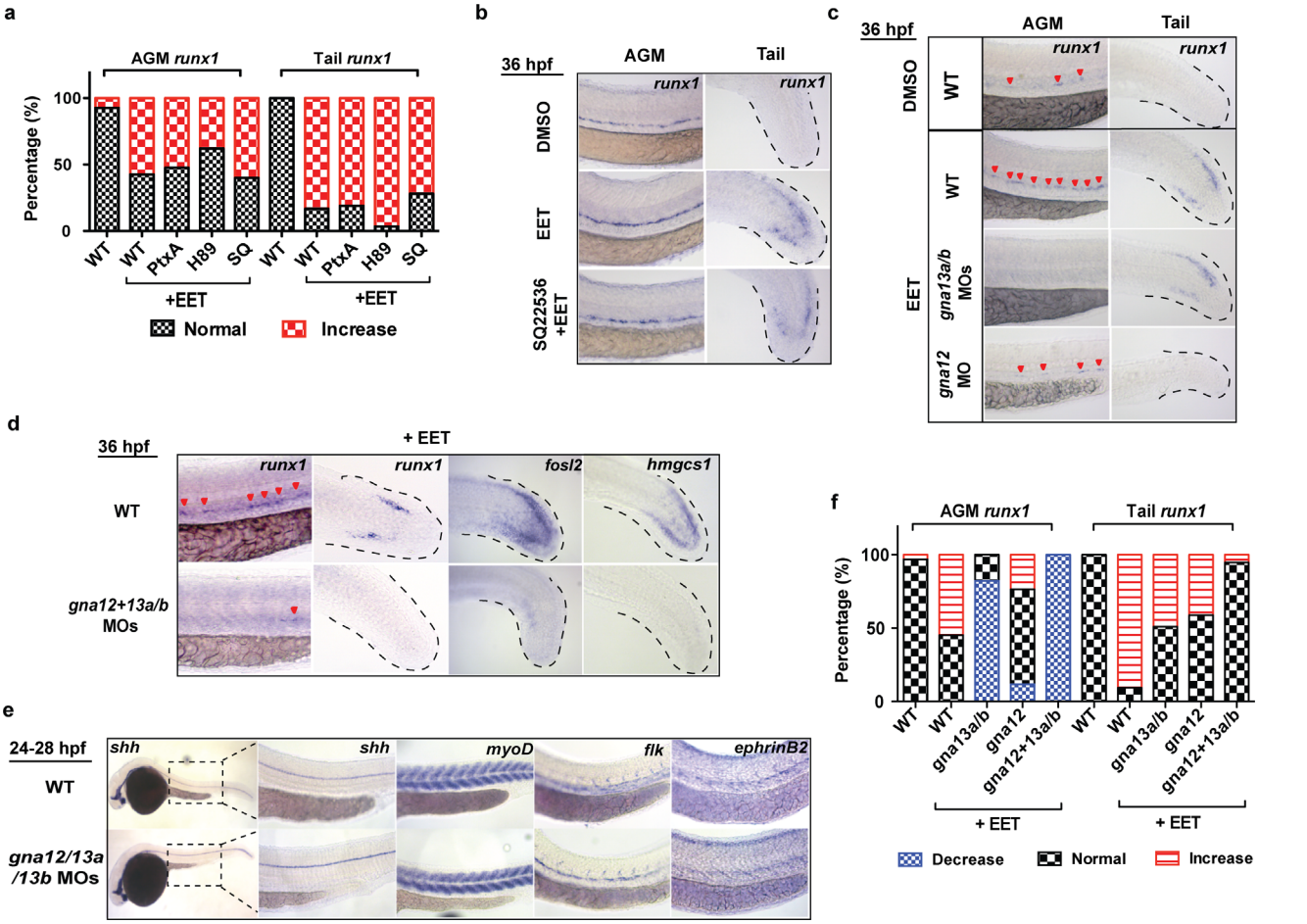

Extended Data Figure 10 | Gα12/13 is specifically required for EET-induced phenotypes in zebrafish embryos. All embryos were treated with DMSO or 5 μM 11,12-EET between 24 and 36 hpf. Chemical inhibitors were added 30 min before EET. mRNA or morpholinos (MO) were injected at the one-cell stage. **a**, **b**, Inhibiting Gαs or Gαi had no effect on EET-induced *runx1* expression. Embryos were categorized into two groups with either normal or increased *runx1* expression level ($n > 20$ each). PtxA, pertussis toxin A, 3 pg, inhibiting Gαi (ref. 30); H89, 5 μM, PKA inhibitor downstream of Gαs[5]; SQ, SQ22536, 50 μM, adenylate cyclase inhibitor downstream of Gαs[5]. Representative images from each group (**b**) (a total of $n > 40$ from two independent experiments). **c**–**f**, Synergistic effects of *gna12/13a/13b* knockdown on suppressing *runx1* expression. Knocking down *gna13a/b* or *gna12* alone partially inhibited EET-induced *runx1* expression in the AGM and tail (**c**). *gna12* MO: 2 ng; *gna13a/13b* MOs: 1 ng each. Triple morpholinos against *gna12*, *gna13a* and *gna13b* (0.67 ng each) completely blocked EET-induced multiple gene expression, including *runx1*, genes in regeneration (*fosl2*) and cholesterol metabolism (*hmgcs1*) (**d**), while other major tissue development processes were not significantly affected, such as notochord (*shh*), muscle (*myoD*), and blood vessels (*flk*, *ephrinB2*) (**e**). **f**, The results were quantified. Embryos were categorized as having decreased, normal or increased *runx1* expression. The bar graph represents the percentage of embryos in each group ($n > 30$).